Chinese Journal of Chemical Engineering 55 (2023) 137–147

Contents lists available at ScienceDirect

Chinese Journal of Chemical Engineering

journal homepage: www.elsevier.com/locate/CJChE

Full Length Article

# A novel high-efficient P/N/Si-containing APP-based flame retardant with a silane coupling agent in its molecular structure for epoxy resin

Qiang Sun [1], Jinlei Wang [1], Xue Meng [1], Jie Zhang [1,2], Hong Yan [1,2,*]

[1] College of Materials Science and Engineering, Taiyuan University of Technology, Taiyuan 030024, China
[2] Key Laboratory of Interface Science and Engineering in Advanced Materials (Taiyuan University of Technology), Ministry of Education, Taiyuan 030024, China

ARTICLE INFO

*Article history:*
Received 16 October 2021
Received in revised form 28 May 2022
Accepted 6 June 2022
Available online 11 June 2022

*Keywords:*
Ammonium polyphosphate
Silane coupling agent
All-in-one system
Flame retardancy
Epoxy resin

ABSTRACT

A flame retardant containing multiple antiflaming elements usually exhibits high-efficient flame retardancy. Here, a novel P/N/Si-containing ammonium polyphosphate derivative (APTES-APP) is synthesized from ammonium polyphosphate (APP) and silane coupling agent (3-aminopropyl)triethoxysilane (APTES) *via* cation exchange, which is quite different in the chemical structure from APTES-modified APP for retaining silicon hydroxyls. APTES-APP is highly efficient for the epoxy resin. 8% (mass) APTES-APP imparts excellent flame retardancy to the epoxy resin, with a V-0 rating at the UL-94 test (1.6 mm) and an LOI value of 26% (vol). The peak heat release rate and total smoke production of the flame-retardant epoxy resin are decreased by 68.1% and 31.3%, respectively. The synergy of P/N/Si contributes to the well-expanded char residue with a strong and dense surface layer, which is a very good barrier against heat and mass transfer. Besides, there is no significant deterioration in the mechanical properties of flame-retardant epoxy resin thanks to silicon hydroxyls forming hydrogen bonds with epoxy molecules. Meanwhile, other molecules can be grafted onto APTES-APP via these silicon hydroxyls, if needed. Briefly, this work has developed a new strategy for amino silane as flame retardants. In conjunction with a low-cost and simple preparation method, APTES-APP has a promising prospect in the high-performance flame-retardant epoxy.


## 1. Introduction

Epoxy (EP) resins are widely used in electronics, aerospace, and high-performance coatings under their excellent mechanical properties, chemical resistance, and durability [1–3]. Whereas pristine epoxy resins are highly combustible, their flame retardancy needs to be improved to reduce fire risk [4–6]. Therefore, it is particularly important to improve the flame retardant properties of EP with suitable techniques while retaining its inherent properties [7].

Among those studies on flame retardants for EP, the popular strategies are structural modification by introducing functional groups with flame retardancy into the molecular structure of EP and blending modification with flame-retardant fillers [8]. Two types of flame retardants are commonly used, nano flame retardants and intumescent flame retardants (IFRs). Nano flame retardants such as nanoclays and other nanocarbon materials enhance flame retardancy based on their geometric hindrance [9–13]. IFRs create a synergistic effect to extinguish fires based on chemical reactions. IFRs consist primarily of inorganic acids or acid sources that produce acids when heated, blowing agents that decompose gases to cause intumescence under the right conditions, and charring agents (CA) [14]. IFRs are non-toxic, non-halogenated materials that are very effective in epoxy resins [8].

Ammonium polyphosphate (APP) has attracted great attention in the field of flame retardants due to its high phosphorus (acid source) and nitrogen (blowing agent) content [15], cost-effectivity, and ease of application in various polymeric matrices [8,16–18]. In the combustion process of resins comprising APP, incombustible gases released from APP can effectively inhibit the gas-phase combustion reaction; nevertheless, in the condensed phase, APP cannot directly provide a CA to form a high-quality insulating char layer, thus its flame retardancy requires improvement with other substances [19]. It is worth noting that the poor compatibility of APP with polymer matrix results in severe deterioration of the mechanical properties [8]. Compared with physical blending [20,21], encapsulation not only promotes the reaction between APP and CA but also improves the compatibility of APP with the matrix [22,23]. Qiu *et al.* [22] prepared a novel multifunc-

* Corresponding author at: College of Materials Science and Engineering, Taiyuan University of Technology, Taiyuan 030024, China.
*E-mail address:* yanhong@tyut.edu.cn (H. Yan).

https://doi.org/10.1016/j.cjche.2022.06.004
1004-9541/

tional organic-inorganic hybrid, melamine-containing polyphosphazene wrapped ammonium phosphate (PZMA@APP) by a polycondensation reaction. PZMA@APP with active amino groups was a highly efficient flame retardant for EP. This hybrid structure presented a multi-functional effect on improving the flame retardant and mechanical performance of EP composites. In addition, grafting small molecules containing flame-retardant elements to APP is much more efficient in the quick formation of a crosslink char during combustion. Kim *et al.* [24] selected 4,40-diaminodiphenylmethane (DDM) as the curing agent and charring agent for the surface modification on the APP, which was applied to epoxy composites. The addition of amine-modified APP (mAPP) accelerated the curing of epoxy composites, contributed to the formation of cross-linked structures, and promoted the formation of compact carbonaceous char structures, so the mechanical properties, thermal degradation, and flame retardancy of the epoxy composites were all improved.

Si-containing flame-retardant structures are more likely to be retained in the condensed phase during burning, thus improving the stability and yield of residues at high temperatures [25]. Therefore, we decide to use a silane coupling agent to achieve this goal. Abundant chemical groups of silane coupling agents offer the possibility to develop our thoughts. Alkoxysilane groups at one end of silane molecules enable reactions on hydroxyl-rich surfaces, and various functional groups (*e.g.*, amino, vinyl, and mercaptan) at the other end are capable of linking to diverse substances [26]. Usually, the silanol groups (Si—OH) formed from alkoxy groups of silane were used to modify the surface of the fillers, improving their compatibility with the polymer matrix [26–28]. In this case, silane serves as a "molecular bridge" at the interface, and its dosage is generally 0.1%–2% (mass) of the filler. In addition, it has been demonstrated that silane-modified APP can enhance the performance of composites in terms of thermal stability and limiting oxygen index, but other synergists are still needed to enhance the flame resistance [29,30]. In this work, however, the silane coupling agent grafts onto APP molecules *via* $—NH_2$ groups that react with $NH_4^+$, while Si—OH groups are kept for dehydration at high temperatures. Importantly, elements P, N, and Si in one molecule are beneficial to the maximum of their synergy.

Herein, (3-aminopropyl)triethoxysilane (APTES) was bonded to APP molecule, forming an all-in-one IFR molecule (APTES-APP) which is highly efficient for epoxy resin (EP) at an 8% (mass) addition. The obtained APTES-APP was characterized by different measurements to confirm its structure, and the flame retardancy and mechanical properties of the EP/APTES-APP composites were investigated. In addition, the corresponding flame-retardant mechanism was discussed.

## 2. Experimental

### 2.1. Materials

Commercial ammonium polyphosphate (APP, $n$ = 1500) was supplied by Hefei WanRan New Material Technology Co., Ltd. (China). (3-Aminopropyl)triethoxysilane (APTES) was purchased from Beijing Chemical Reagents Co., Ltd. (China). Sodium hydroxide (NaOH, AR), ethylene glycol (AR), and absolute ethyl alcohol (AR) were received from Tianjin DaMao Chemical Reagents Factory Co., Ltd. (China). Epoxy resin (E-44) and a polyamide curing agent (651) were obtained from Jinan TianMao Resin Chemical Co., Ltd (China).

### 2.2. Synthesis of APTES-APP

At room temperature, 70 ml of sodium hydroxide solution (NaOH, 0.5 mol·$L^{-1}$) was mixed well with 420 ml of ethylene glycol under continuous stirring. Afterward, APTES (16.8 ml) and APP (7 g) were added sequentially. The reaction system was kept stirred at 600 r·$min^{-1}$, 50 °C for 5 h. After vacuum filtration, APTES-APP powder was obtained after being rinsed with ethanol three times and then dried under vacuum at 80 °C. The synthesis mechanism of APTES-APP is shown in Fig. 1.

### 2.3. Preparation of EP composites

First, 8.00 g of APTES-APP and 61.34 g of EP were homogenized in a dispersion machine at 1500 r·$min^{-1}$. Next, 30.66 g of polyamide curing agent was put into the previous mixture and stirred

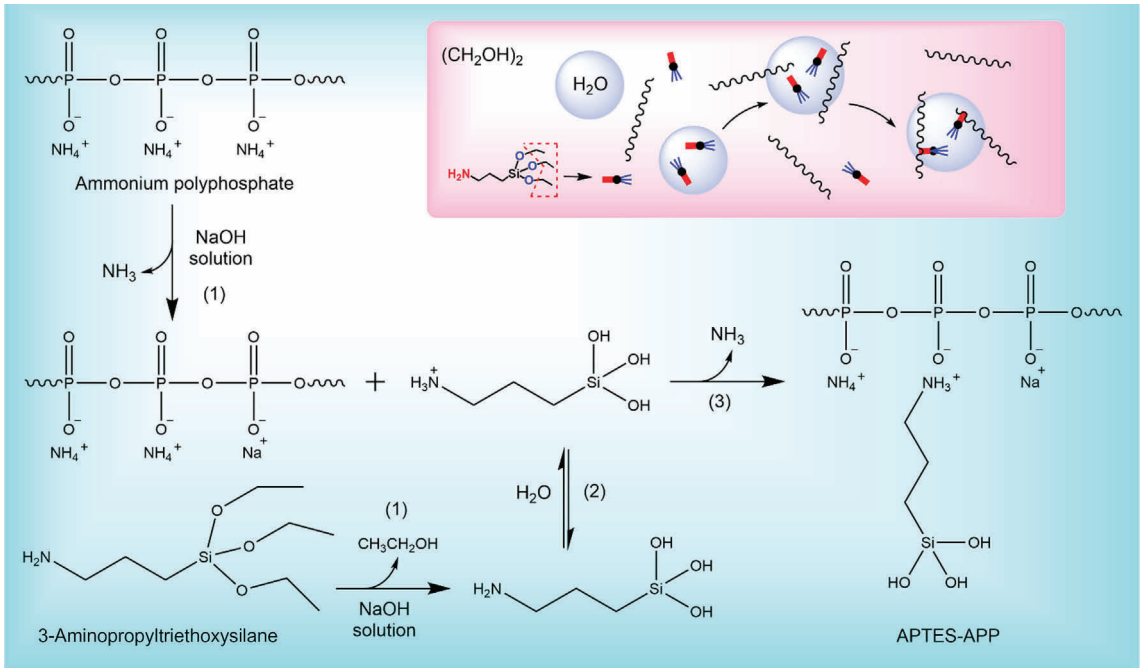


**Fig. 1.** The synthetic route of APTES-APP.

for 10 min. Lastly, the resulting mixture was poured into different preheated molds. The specimens were cured at room temperature for 2 h and then at 80 °C for another 3 h. Additionally, EP and EP/APP were prepared as control specimens. The relevant formulations are listed in Table 1.

### 2.4. Characterization and testing

Fourier transform infrared (FTIR) spectra were recorded by a Nicolet-710 spectrometer (Nicolet, America) using the KBr disk. X-ray diffraction (XRD) was employed on an X-ray diffractometer (X'Pert PRO MPD, Holland), using Cu $K_\alpha$ radiation ($\lambda$ = 0.15418 n m), at a scanning rate of 4 (°)·min$^{-1}$. X-ray photoelectron spectroscopy (XPS) spectra were monitored by an ESCALAB 250 XI (Thermo Scientific, America) using Al $K_\alpha$ excitation radiation ($h\nu$ = 1486.6 eV). The surface morphologies of the samples were observed by a JEOL JSM 5900 L V scanning electron microscopy (SEM) (JEOL, Japan) at the accelerating voltage of 15 or 200 kV. The particle size and particle size distribution of the powders were tested using a laser particle sizer (Mastersizer 3000, United Kingdom). Thermogravimetric analysis (TGA) was carried out on an STA-409 thermal analyzer (Netzsch, Germany), at a heating rate of 10 °C·min$^{-1}$ under the nitrogen flow of 50 ml·min$^{-1}$ in the temperature range from room temperature to 800 °C.

The limiting oxygen index (LOI) values were tested on a digital oxygen index meter (ZR-01, China) with sheet dimensions of 125 mm × 10 mm × 4 mm according to ASTM D2863-19. The UL-94 vertical burning level was measured on an instrument (JR-SSC-A, China) according to ASTM D3801-19, and the dimension of all specimens was 125 mm × 13 mm × 1.6 mm. The LOI values and UL-94 ratings of each sample were repeated 5 times. The tensile properties of the EP composites were measured at room temperature using an electronic tensile tester (RH-10kN, China) at an extension rate of 1 mm·min$^{-1}$ following the test standard ASTM D638-14. The notched impact behavior was measured with a cantilever beam impact tester (RH-6050, China) in line with ASTM D256-10 with a sample size of 10.2 mm × 12.7 mm × 3.2 mm. Samples for both tensile and impact tests were operated five times and the average values were reported. Cone calorimeter tests (CCT) were employed to investigate the fire performance of EP and its composites based on ISO5660-1: 2015, the specimens (100 mm × 100 mm × 3 mm) were measured horizontally under a heat flux of 50 kW·m$^{-2}$ and three specimens were tested for each formulation. The volatile gases produced during the thermal degradation of specimens were tested using a thermogravimetric analyzer (STA-409, Germany) and a Fourier transform infrared spectroscopy (Nicolet-710) at a heating rate of 10 °C·min$^{-1}$ under a nitrogen flow of 20 ml·min$^{-1}$. Laser Raman spectroscopy measurement was carried out at room temperature with Lab RAM HR800 laser Raman spectrometer (SPEXCo, America) using a 514 nm argon-ion laser.

## 3. Results and Discussion

### 3.1. Characterization of APTES-APP

APP of a low and high degree of polymerization were both used in this work. The former is soluble in hot water, making the preparation convenient. But 10% (mass) of the synthesized compound did not have EP pass V-0 rating at UL-94 test. It can be inferred that low degree polymerized APP is of low thermal stability. So high thermal-stable APP ($n$ = 1500) was selected to prepare APTES-APP. NaOH solution was employed to promote the dissolution of APP for the homogeneous reaction [31]. Simultaneously, APTES rapidly hydrolyzed in an alkaline environment to form silanols [32]. The presence of ethylene glycol aimed to avoid the self-condensation of silanols, thus ensuring silanols were retained in APTES-APP molecules. When NaOH was gradually consumed by APP, the silanols took the chance to be protonated, and then APTES-APP formed via ion exchange with $NH_4^+$ [24,33–35].

The APP and the resulting product were subsequently characterized. APTES-APP has similar FTIR spectra as APP except for new characteristic peaks of the asymmetric deformation of $NH_3^+$ (1665–1600 cm$^{-1}$) and stretching of —OH (3645–3300 cm$^{-1}$) (Fig. 2(a)) [17,24,36]. The wide-scan spectra of XPS show that APTES-APP contains Si and Na elements that are not found in APP (Fig. 2(b)). Besides, the N 1s spectrum of APP only contains $NH_4^+$ (401.5 eV) and —P—NH—P— (399.6 eV), while that of APTES-APP presents a new peak at 400.9 eV belonging to N—H in $NH_3^+$ (Fig. 2(c), (f)) [36]. The binding energy in the O 1s spectrum of APTES-APP near 534.9 eV corresponds to the O in Si—OH (Fig. 2(d), (e)) [37]. These sufficiently demonstrate the APTES-APP is in line with the expected target structure shown in Fig. 1. Fig. S1 (in Supplementary Material) shows a wide distribution of particle sizes of APP and APTES-APP, both ranging from 3 to 110 μm. Their volume average particle sizes are close, APTES-APP (25.6 μm) and APP (26.8 μm).

The SEM images of APP and APTES-APP show no great difference in their morphologies (Fig. 2(g), (i)); the energy dispersive spectrometer (EDS) mappings exhibit that APTES-APP contains elements P and N from APP, as well as element Si from APTE, and element Si are uniformly distributed between P and N (Fig. 2(h), (j)). Furthermore, a new small diffraction peak (in the circle) appears in the XRD pattern of APTES-APP (Fig. 2(k)), and the other peaks remain the same as those of APP, suggesting no big change in crystalline structure for these two. It is observed from TG curves (Fig. 2(l)) that APTES-APP and APP begin to decompose at 300 °C. APTES-APP starts to cleave slightly earlier than APP, probably because of an earlier release of ammonia and the silanols dehydration. At 800 °C, however, the residue of APTES-APP is 10% heavier than that of APP.

### 3.2. Mechanical properties of EP and its composites

It is well-known that flame-retardant fillers may cause damage to the mechanical properties of polymers [38]. Therefore, the tensile strength and impact strength of EP composites were tested (Fig. 3), and the results are listed in Table 2. Fig. 3(a) indicates that the tensile strength of EP/APP is 37.6 MPa, with a 16.1% decrease compared to that of pure EP. While EP/APTES-APP has a 5.8% increase in the tensile strength compared to EP/APP. The impact strength of EP/APTES-APP is 3.4% greater than that of pure EP (Fig. 3(b)). This slight improvement can be attributed to the Si—OH in APTES-APP improving its compatibility with the EP matrix *via* hydrogen bonds.

**Table 1**
The formulations of IFR-EP and the LOI and UL-94 results

| Item | Epoxy resin/g | Curing agent/g | APP/g | APTES-APP/g | LOI /% (vol) | UL-94 (1.6 mm) |
|---|---|---|---|---|---|---|
| EP | 61.34 | 30.66 | – | – | 18.2 | No rating |
| EP/APP | 61.34 | 30.66 | 8 | – | 25.2 | No rating |
| EP/APTES-APP | 61.34 | 30.66 | – | 8 | 26.0 | V-0 |

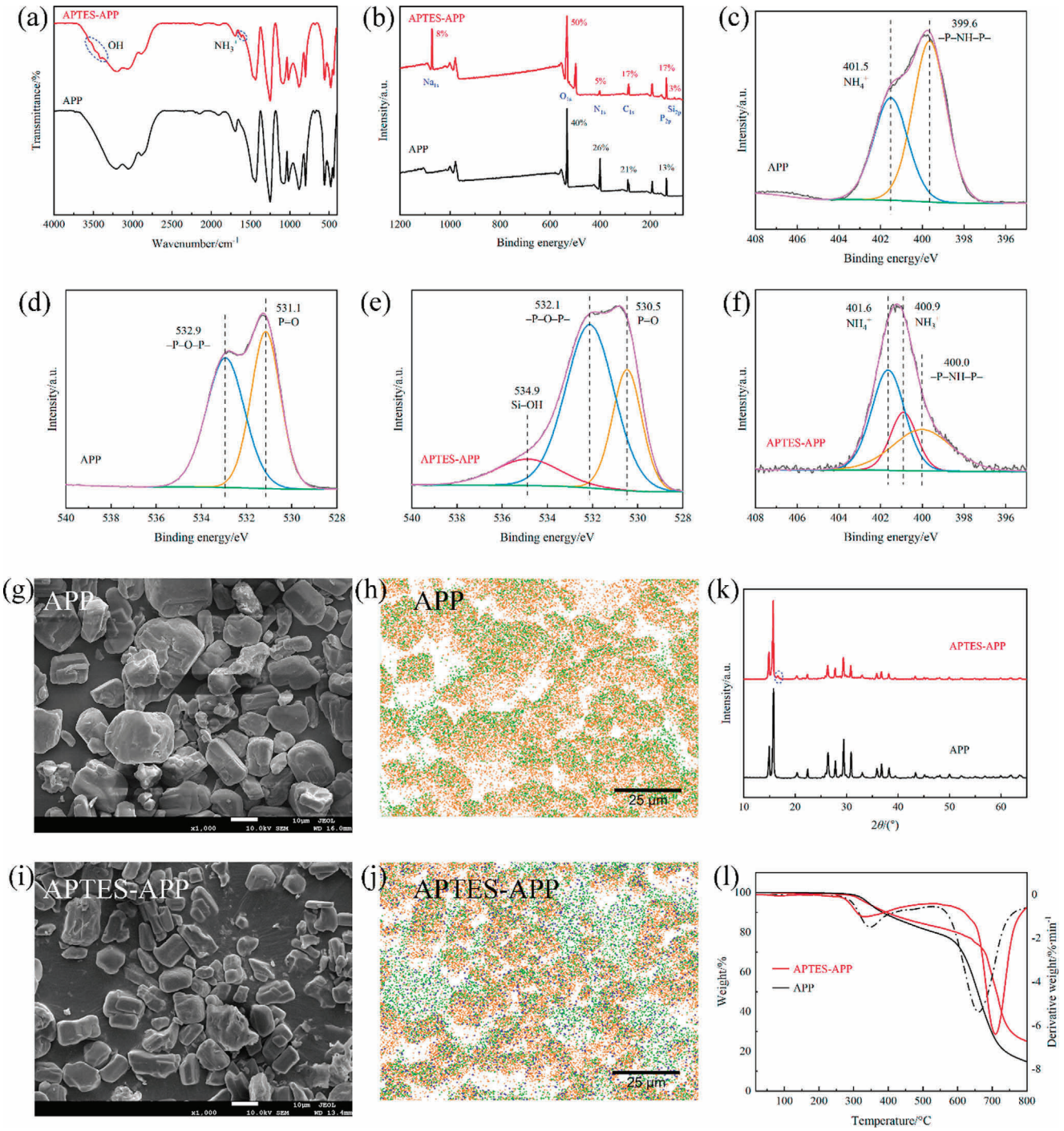


**Fig. 2.** FTIR spectra (a), XPS spectra (b–f), SEM images (g, i), EDS mapping (h, j) (orange-P, green-N, blue-Si), XRD patterns (k), and TG curves (l) of APP and APTES-APP.

The FTIR spectra of EP and EP/APTES-APP (Fig. 4(a)) show that some characteristic peaks of EP, including the hydroxyl (—OH) peak at 3410 $cm^{-1}$, the C—N peak of tertiary amide at 1245 $cm^{-1}$, and the out-of-plane bending peak at 940 $cm^{-1}$ attributed to carboxylic acid C—OH from curing agent, are changed after the addition of APTES-APP to EP. This is because of hydrogen bonds formed between the EP matrix and the Si—OH of APTES-APP. The cross-section micromorphology of the EP/APTES-APP after the tensile strength test (Fig. 4(b)) further demonstrates the good dispersity and compatibility of APTES-APP in the EP matrix, with no aggregation and obvious gaps around particles (holes left by particle pullout). SEM images of fractured surfaces of EP and EP/APP (Fig. S2) exhibit that the fractured surface of pure EP is relatively smooth, but the fractured surface of EP/APP is very rough and has some aggregation of particles. That is why the mechanical properties of EP/APTES-APP are better than those of EP/APP.

### 3.3. Flame retardancy of EP and its composites

The flame resistance of EP composites is evaluated by the limiting oxygen index (LOI) and UL-94 vertical burning level as shown in Table 1. EP is flammable, with an LOI value of 18.2 %(vol) and no UL-94 rating (Fig. S3(a)). With 8% (mass) of APP added, the LOI value of EP/APP increases to 25.2% (vol), but the UL-94 test

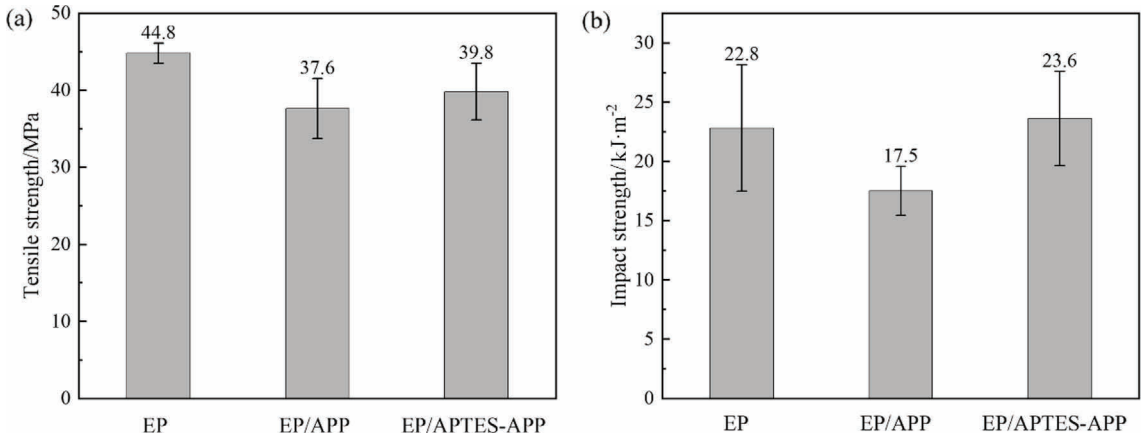


**Fig. 3.** The tensile (a) and impact (b) strengths of EP, EP/APP, and EP/APTES-APP.

**Table 2**
Mechanical parameters of EP, EP/APP, and EP/APTES-APP

| Items | EP | EP/APP | EP/APTES-APP |
|---|---|---|---|
| Tensile strength/MPa | 44.8 ± 1.3 | 37.6 ± 3.9 | 39.8 ± 3.7 |
| Impact strength/kJ·m$^{-2}$ | 22.8 ± 5.3 | 17.5 ± 2.1 | 23.6 ± 4.0 |

result is still disappointing (Fig. S3(b)). At the same loading of 8% (mass), APTES-APP enhances the LOI value of EP to 26.0% (vol), and the UL-94 rating achieves the V-0 level (Fig. 5). 8% (mass) is the lowest loading amount for EP/APTES-APP passing the V-0 rating.

Cone calorimetry testing (CCT) is widely used for fire hazard assessment of engineering plastics during real combustion conditions [39,40]. It can provide useful information related to fire, such as heat release, mass loss, smoke, *etc.* Therefore, EP/APTES-APP was taken to conduct a controlled trial on CCT with EP and EP/APP (Video S1). The curves of heat release rate (HRR), total heat release (THR), mass loss (ML), smoke production rate (SPR), and total smoke production (TSP) are illustrated in Fig. 6. The detailed CCT results are presented in Table 3.

The peak of HRR (PHRR) and THR are key parameters of the flame propagation capability in a fire, so their reduction is critical for fire safety [41]. According to Fig. 6 and Table 3, for pure EP, the time to ignition (TTI) is 28 s, the PHRR (1085.4 kW·m$^{-2}$) is at 105 s, and the THR at the end is 91.1 MJ·m$^{-2}$. While the TTI and the time to PHRR (tPHRR) of EP/APTES-APP are delayed by 9 s and 25 s, and its PHRR and THR are reduced by 68.1% and 34.0%, respectively. All these performances of EP/APP are inferior to those of EP/APTES-APP.

The fire growth rate index (FIGRA = max [HRR($t$)/$t$]) is usually used for predicting the degree of fire danger [19,42]. The FIGRA for EP/APP and EP/APTES-APP decreases to 4.51 and 3.80 kW·m$^{-2}$·s$^{-1}$, respectively, far below 10.34 kW·m$^{-2}$·s$^{-1}$ for EP. It should be known that a lower FIGRA value means that people have more time to escape from the fire field. Besides, the ML curves further prove that EP/APTES-APP is superior to EP/APP. Besides heat, smoke is also an important factor that threatens human life in a fire [43]. EP/APTES-APP exhibits stronger smoke suppression than EP/APP, with a 44.2% reduction in PSPR and 31.3% in TSP compared to EP. In a word, EP/APTES-APP performs well in fire and smoke suppression.

### 3.4. Char residue of EP/APTES-APP composite

The intumescent and dense char layer can isolate the heat and oxygen transfer between its surface and bottom, which is significant to improve the flame-retardant efficiency [44]. The digital photographs of residues of EP, EP/APP, and EP/APTES-APP are shown in Fig. 7. EP burned out with little residue left. EP/APP expanded vertically up to 3.2 cm, but its surface was full of holes that did not cut off the inward transfer of heat and oxygen. But

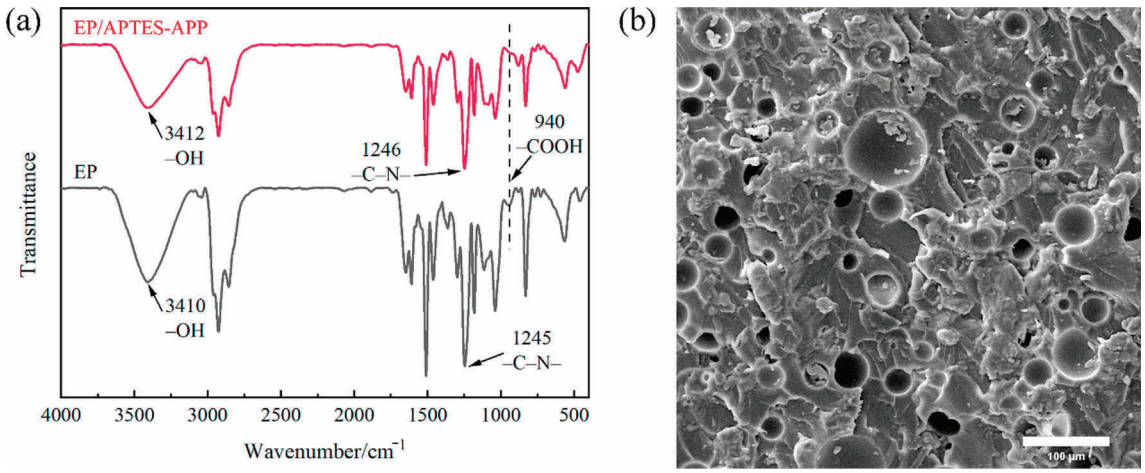


**Fig. 4.** FTIR spectra (a) of EP and EP/APTES-APP and the micromorphology of the cross-section for EP/APTES-APP (b).

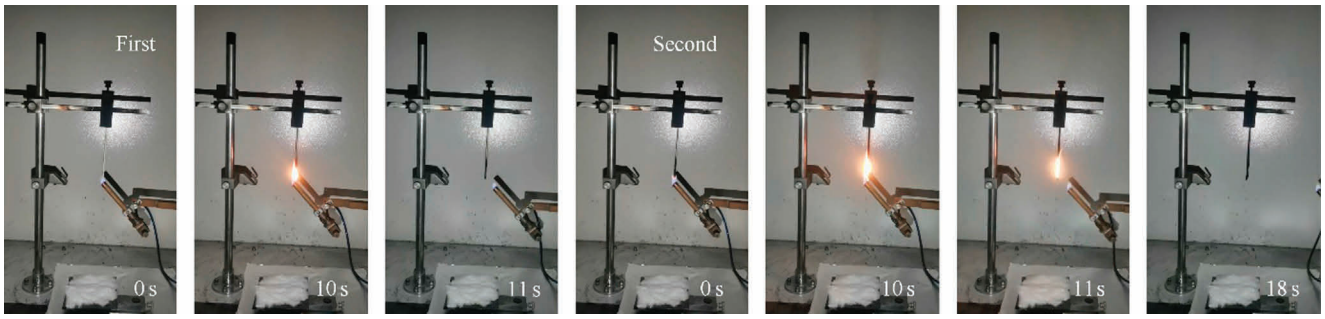


**Fig. 5.** The digital photos of EP/APTES-APP at the UL-94 test.

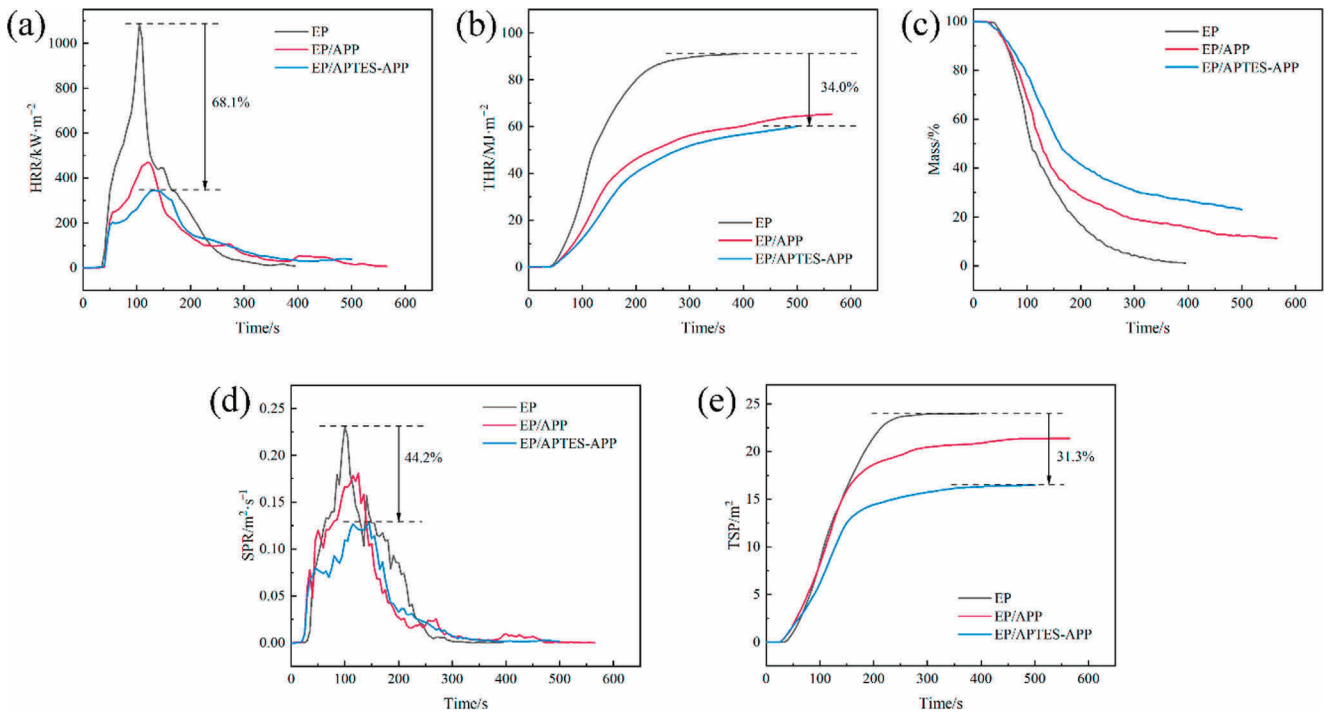


**Fig. 6.** HRR, THR, ML, SPR, TSP curves of EP, EP/APP, and EP/APTES-APP.

**Table 3**
CCT data of EP, EP/APP, and EP/APTES-APP

| Item | TTI /s | PHRR /kW·m$^{-2}$ | tPHRR /s | THR /MJ·m$^{-2}$ | PSPR /m$^2$·s$^{-1}$ | TSP /m$^2$ | Residue /% (mass) | FIGRA /kW·m$^{-2}$·s$^{-1}$ |
|---|---|---|---|---|---|---|---|---|
| EP | 28 | 1085.4 | 105 | 91.1 | 0.231 | 23.9 | 1.0 | 10.34 |
| EP/APP | 30 | 469.3 | 120 | 65.0 | 0.181 | 20.8 | 11.3 | 4.51 |
| EP/APTES-APP | 37 | 345.7 | 130 | 60.1 | 0.129 | 16.5 | 23.0 | 3.80 |

for EP/APTES-APP, it expanded too high beyond the upper frame of the instrument, so the top of the char residue was chipped off while being moved out (Video S2). Even so, the height of char without the top layer reached 6.5 cm, twice higher than that of EP/APP. This suggests that the top surface layer was compact enough to hold more gases inside. Moreover, the well-expanded char was so strong without getting broken when the bottom was turned over, as shown in the rightmost photograph.

SEM images and Raman spectra (Fig. 8) of char residue from EP/APTES-APP after CCT further demonstrate its high-quality microstructure. Surprisingly, SEM images (Fig. 8(a), (b)) exhibit that the surface and bottom char layers are pretty compact, continuous, and smooth, which are distinct from reported literature about the APP-based flame retardant system. As shown in Fig. S4 (a), (b), the microstructure of the char residue of EP/APP after CCT is full of pores, which can not well insulate from heat and oxygen transfer. Raman spectra (Fig. 8(c), (d)) serve to characterize the order degree of chars, and these spectra show two characteristic bands: D-band (about 1366 cm$^{-1}$, caused by the vibrations of amorphous char) and G-band (about 1590 cm$^{-1}$, caused by the vibrations of sp2-hybridized carbons) [45–47]. The degree of graphitization of chars can be measured by the ratio of the integrated intensity of D- and G-band ($I_D/I_G$); the lower the $I_D/I_G$ value, the higher the degree of graphitization of the char. Graphitized char is an excellent flame-retardant barrier that facilitates fire retardation [48]. For EP/APTES-APP, the $I_D/I_G$ values of the surface

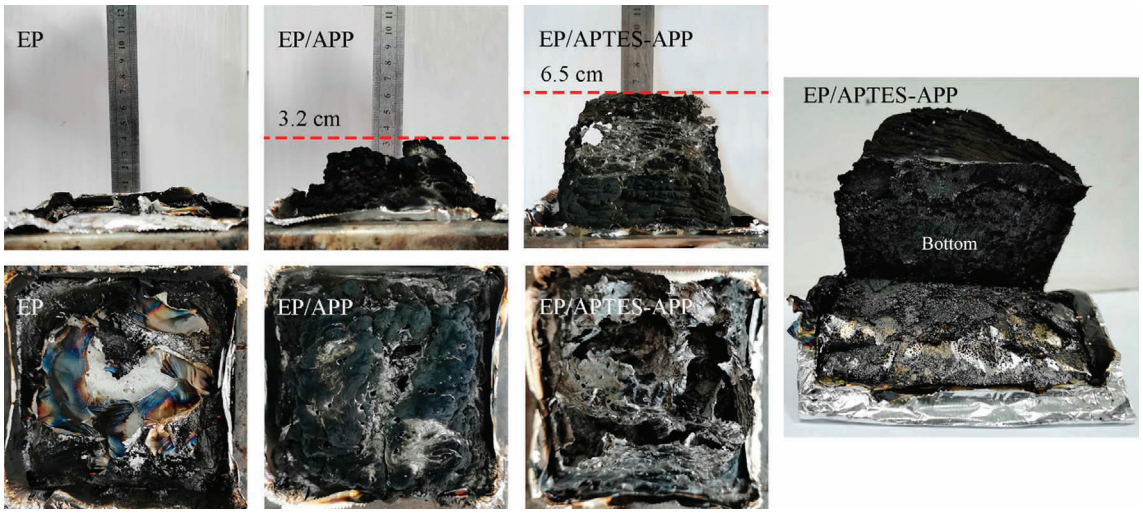


**Fig. 7.** Digital photographs of char residues of EP, EP/APP, and EP/APTES-APP (the rightmost one showing the bottom up).

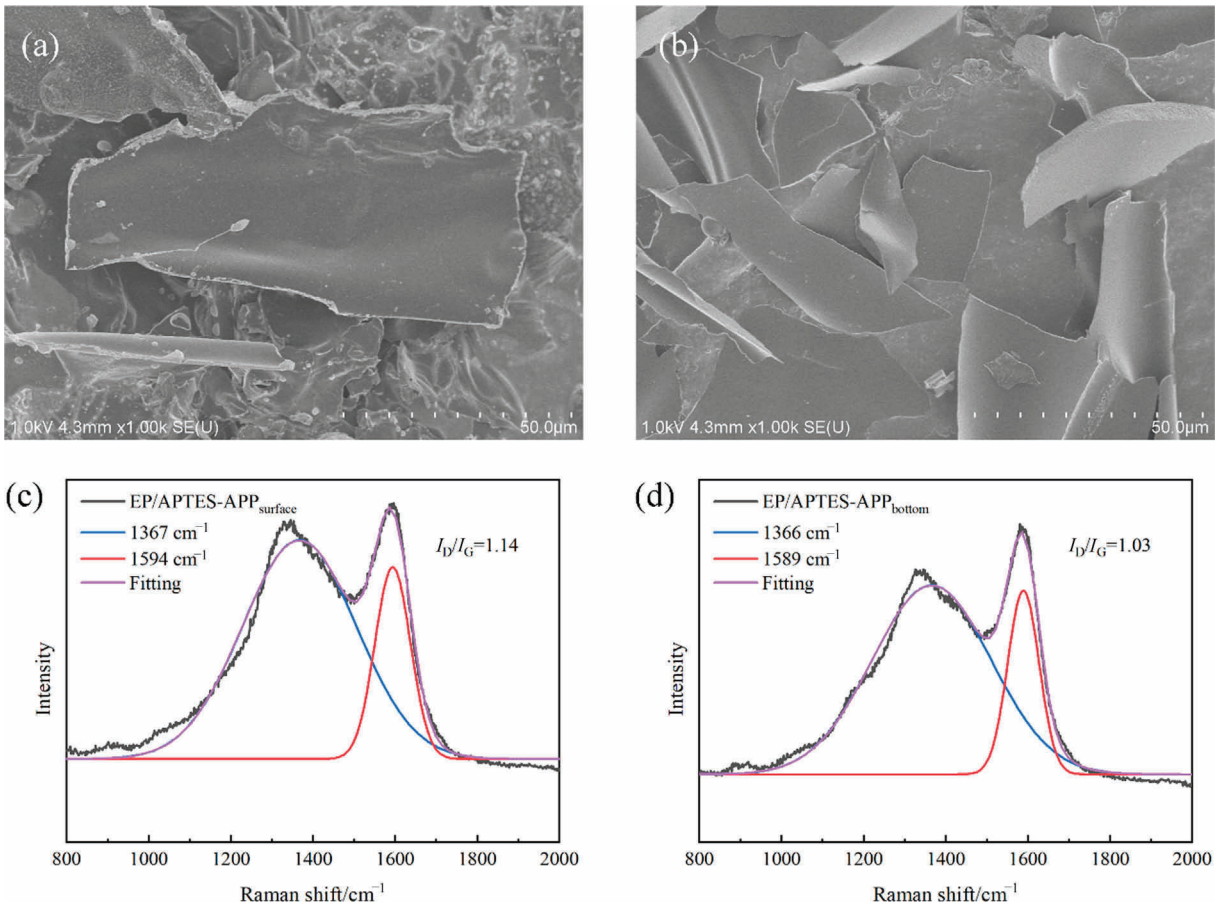


**Fig. 8.** SEM images and Raman spectra of char residues of EP/APTES-APP after CCT (surface: (a), (c); bottom: (b), (d)).

and bottom char layers are 1.14 and 1.03 (Fig. 8(c), (d)), while these values are 1.22 and 1.24 for EP/APP (Fig. S4(c), (d)). Therefore, APTES-APP enhances the degree of graphitization of char, having better performance in the condensed phase than APP. Si element may contribute to the formation of high-quality char, which cuts off the heat and mass transfer and provides excellent fire protection for EP resin.

### 3.5. Flame retardant mechanism

XPS spectra are available to detect the composition of char residue to illustrate the mechanism of char formation (Fig. 9). In the C 1s spectra, peaks near 284.7 eV are attributed to aliphatic C—C/C—H and aromatic C=C, while peaks at 286.1, 288.3, and 291.4 eV are assigned to C—O—C, O—C=O, and plasmon, respec-

tively [49–51]. The peak of C—Si (284.4 eV) appears in the $C_{1s}$ spectrum; likewise, Si—C is observed in the Si 2p spectrum at 102.0 eV [19]. Although the Si content in char is low, the Si—O (103.1 eV) peak can still be easily identified in Si 2p spectra [49,52,53]. The P 2p peak at 134.5 eV is attributed to $PO_4^-$. In conjunction with the peak of $NH_3^+$ at 401.1 eV and —P—NH—P— at 399.7 eV in $N_{1s}$ spectra of the bottom, it is reasonable to believe that the effective components of APTES-APP still stay in the bottom residue. As a result of sustained irradiation, Si—N (398.5 eV) in the $N_{1s}$ spectrum and O=P—O—C (134.7 eV) in the P 2p spectrum indicate more cross-linked structures forming in the upper char [54,55]. These can be supported by the O 1s spectra. While P—O—P and P=O dominate the O 1s spectrum of the bottom char, the C—O—C structure is visible in the surface residue because of the gradual decomposition

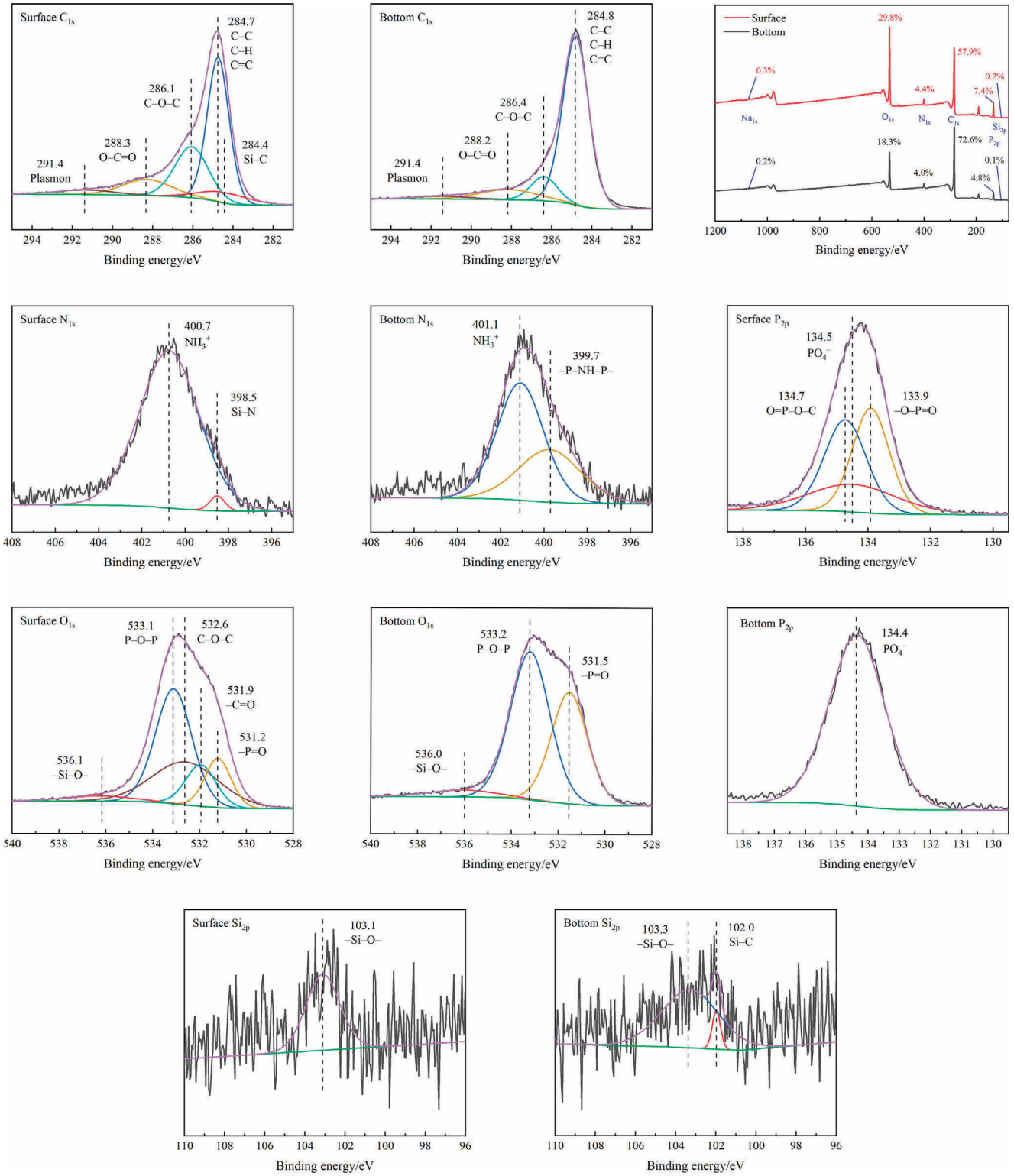


**Fig. 9.** The wide-scan, C 1s, N 1s, O 1s, P 2p, and Si 2p XPS spectra of char residues of EP/APTES-APP after CCT.

of phosphate. Besides, the —Si—O— (536.1 eV) structure is also present in O 1s spectra, resulting from the dehydration cross-linking of Si—OH in APTES-APP. It is noteworthy that the peak at 531.9 eV in the O 1s spectrum of the surface char is ascribed to the carbonate C═O while Na is the only metallic element present in chars, and this suggests some sodium carbonate ($Na_2CO_3$) generating in the process [56]. Both the Si—O structure and $Na_2CO_3$ are essential for making glass, which may explain the strong char residue of EP/APTES-APP with a microscopic "glassy" appearance [57]. Furthermore, the discussion on the FT-IR spectra of char residue from EP/APTES-APP after CCT proves the crosslinking structure: P—O—C/Si—O—Si/Si—O—P/Si—C/Si—N char residues (Fig. S5).

To further illustrate the flame-retardant mechanism, the pyrolysis of different samples was studied using thermogravimetric-infrared (TG-IR) analysis, as shown in Fig. 10. The initial decomposition temperature (at 5% mass loss, $T_{5\%}$), the temperature of maximum decomposition rate ($T_{max}$), and char yield (CY) at 800 °C are listed in Table 4. To avoid the interference of oxygen and other air impurities, the samples underwent pyrolysis in a nitrogen flow. In the TG-DTG curves (Fig. 10(a)), EP/APTES-APP and EP/APP degrade before pure EP at about 310 °C because the flame retardants start to decompose. Over 500 °C, the samples' residual weights tend to be stable. EP almost has nothing left, while EP/APTES-APP and EP/APP retain about 13% (mass) of residues. In the range of 250–400 °C, EP/APTES-APP and EP/APP are in the first stage of decomposition. Since APTES-APP and APP start to decompose at 300 °C, the degradation of the EP matrix is triggered in advance. The FTIR spectra of the pyrolysis gaseous products (Fig. 10(b), (c), (d)) further reveal that water vapor (3500–4000 $cm^{-1}$) and ammonia (930–970 $cm^{-1}$) are detected at around 300 °C for EP/APTES-APP, while the corresponding peaks appear at around 350 °C for EP/APP [55,58]. It is because APTES-APP starts the cleavage slightly earlier than APP, releasing ammonia and undergoing the Si—OH dehydration condensation reaction. Then at around 350 °C, EP/APTES-APP again produces P═O (1258 $cm^{-1}$) volatiles earlier than EP/APP, which are considered as free radical scavengers with excellent quenching effect on flame suppression in the gas phase [59,60]. Subsequently, from 400 to 500 °C, EP/APTES-APP and EP/APP enter the second stage of decomposition. The DTG curve of EP/APTES-APP exhibits more variation at this stage, suggesting that it has diverse cleavage routes. The characteristic signals of other pyrolysis gaseous products of the EP matrix are also recorded. These products are easily identified by their characteristic absorbances, such as alkanes (2800–3000 $cm^{-1}$), $CO_2$ (2200–2400 $cm^{-1}$), phenyl (1500 and 1600 $cm^{-1}$), aldehyde RCHO (1172 $cm^{-1}$), and $NH_3$ (827 $cm^{-1}$) [61,62].

Based on the above discussion, we propose a possible flame retardancy mechanism of APTES-APP, as shown in Fig. 11. APTES-APP first releases trace amounts of $H_2O$ from silicon hydroxyl groups and $NH_3$ by thermal decomposition, followed by the formation of polyphosphoric acid. During the dehydration and the release of $NH_3$, a lot of cross-linked structures form "glassy" char,

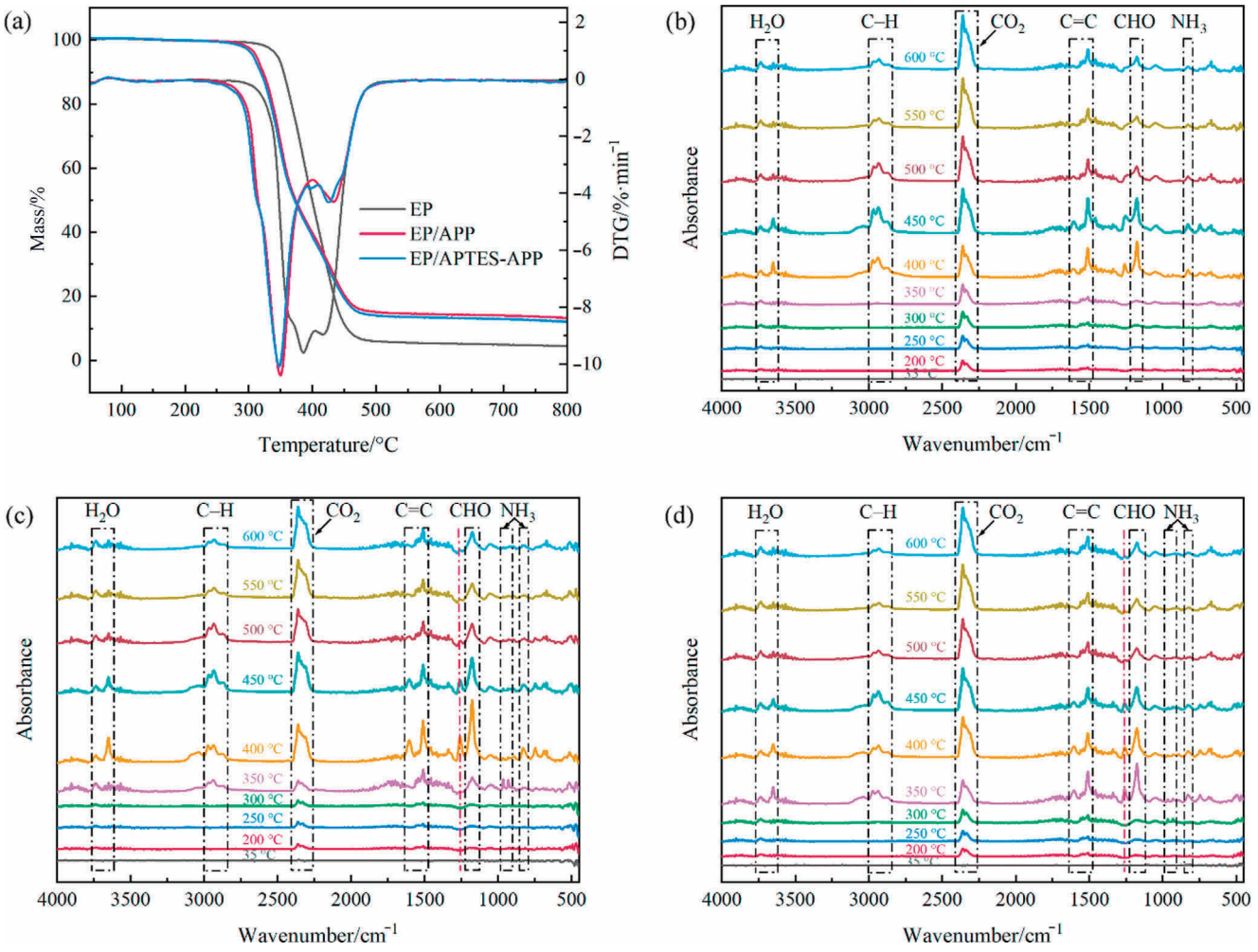


**Fig. 10.** TG, DTG curves (a) and FTIR spectra of gaseous products released from EP (b), EP/APP (c), and EP/APTES-APP (d) at different temperatures during the thermal degradation.

**Table 4**
TGA results of EP and its composites from the TG-IR test

| Item | $T_{5\%}$/°C | $T_{max1}$/°C | $T_{max2}$/°C | CY/% (mass) |
|---|---|---|---|---|
| EP | 345 | 386 | – | 4.5 |
| EP/APP | 312 | 349 | 433 | 13.1 |
| EP/APTES-APP | 307 | 348 | 425 | 12.0 |

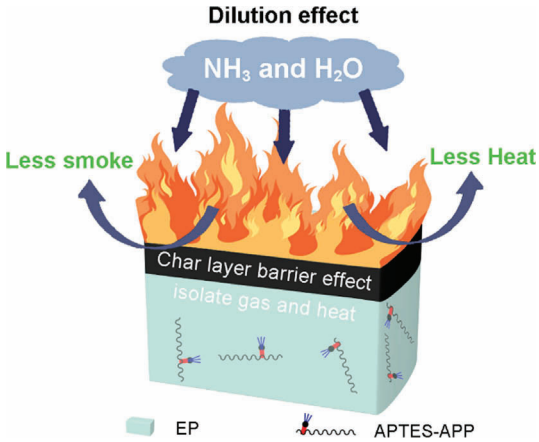


**Fig. 11.** The flame retardancy mechanism of APTES-APP.

including Si—O—Si, Si—O—P, P—O—C, Si—C, and Si—N. The advanced decomposition of APTES-APP contributes to the rapid formation of the char layer [63]. A highly cross-linked strong char layer serves as a good barrier for heat and mass transfer. Simultaneously, $CO_2$, $H_2O$, and $NH_3$ generated from the system dilute the oxygen concentration around the char layer [64]. Therefore, the combined effects in the gaseous and condensed phases inhibit the combustion, suppress the smoke generation, and keep more char residue left.

## 4. Conclusions

In summary, APTES-APP intumescent flame retardant with active Si—OH groups was prepared based on the cation exchange reaction of —$NH_2$ in silane coupling agent APTES with APP. With 8% (mass) of APTES-APP, EP/APTES-APP exhibits an all-round improvement in the flame retardancy in comparison with pure EP, with the V-0 rating at UL-94 test, the LOI value up to 26.0% (vol), 68.1% and 31.3% decreases in PHRR and TSP, and longer time to ignition. The APTES-APP containing P, N, and Si can play three roles (acid source, blowing agent, and charring agent) in one molecule, and the formed high-quality intumescent char layers can effectively protect the underlying material. Moreover, the retained Si—OH groups can improve the compatibility of APTES-APP with EP by hydrogen bonds. Interestingly, this all-in-one APTES-APP can not only be used alone as a flame retardant but also serve as an intermediate to prepare new flame retardant by using its Si—OH groups.

## Data Availability

No data was used for the research described in the article.

## Declaration of Competing Interest

The authors declare that they have no known competing financial interests or personal relationships that could have appeared to influence the work reported in this paper.

## Acknowledgements

This work was financially supported by the National Natural Science Foundation of China (22178242).

## Supplementary Material

Supplementary data to this article can be found online at https://doi.org/10.1016/j.cjche.2022.06.004.

## References

[1] F.L. Jin, X. Li, S.J. Park, Synthesis and application of epoxy resins: A review, *J. Ind. Eng. Chem.* 29 (2015) 1–11.
[2] X.W. Li, Q.Y. Yu, X. Chen, Q.X. Zhang, Microstructures and electrochemical behaviors of casting magnesium alloys with enhanced compression strengths and decomposition rates, *J. Magnes. Alloys* (2021), https://doi.org/10.1016/j.jma.2021.07.018.
[3] X.W. Li, J.S. Liang, T. Shi, D.N. Yang, X.C. Chen, C.W. Zhang, Z.H. Liu, D.Z. Liu, Q.X. Zhang, Tribological behaviors of vacuum hot-pressed ceramic composites with enhanced cyclic oxidation and corrosion resistance, *Ceram. Int.* 46 (9) (2020) 12911–12920.
[4] M. Rajaei, N.K. Kim, S. Bickerton, D. Bhattacharyya, A comparative study on effects of natural and synthesised nano-clays on the fire and mechanical properties of epoxy composites, *Compos. B Eng.* 165 (2019) 65–74.
[5] S.Q. Huo, S. Yang, J. Wang, J.W. Cheng, Q.Q. Zhang, Y.F. Hu, G.P. Ding, Q.X. Zhang, P.G. Song, A liquid phosphorus-containing imidazole derivative as flame-retardant curing agent for epoxy resin with enhanced thermal latency, mechanical, and flame-retardant performances, *J. Hazard. Mater.* 386 (2020) 121984.
[6] Q.Y. Liu, D.H. Wang, Z.K. Li, Z.F. Li, X.L. Peng, C.B. Liu, Y. Zhang, P.L. Zheng, Recent developments in the flame-retardant system of epoxy resin, *Materials* 13 (9) (2020) 2145.
[7] C. Ma, S.L. Qiu, B. Yu, J.L. Wang, C.M. Wang, W.R. Zeng, Y. Hu, Economical and environment-friendly synthesis of a novel hyperbranched poly (aminomethylphosphine oxide-amine) as co-curing agent for simultaneous improvement of fire safety, glass transition temperature and toughness of epoxy resins, *Chem. Eng. J.* 322 (2017) 618–631.
[8] J. Alongi, Z.D. Han, S. Bourbigot, Intumescence: Tradition versus novelty. A comprehensive review, *Prog. Polym. Sci.* 51 (2015) 28–73.
[9] H. Kim, J.W. Park, H.J. Kim, Flame retardant nano-composites containing nano-fillers (in Science and Applications of Tailored Nanostructures), One Central Press, 2017.
[10] H.L. Qin, S.M. Zhang, C.G. Zhao, G.J. Hu, M.S. Yang, Flame retardant mechanism of polymer/clay nanocomposites based on polypropylene, *Polymer* 46 (19) (2005) 8386–8395.
[11] M.L. Du, B.C. Guo, D.M. Jia, Thermal stability and flame retardant effects of halloysite nanotubes on poly(propylene), *Eur. Polym. J.* 42 (6) (2006) 1362–1369.
[12] A. Kausar, I. Rafique, B. Muhammad, Significance of carbon nanotube in flame-retardant polymer/CNT composite: A review, *Polym. Plast. Technol. Eng.* 56 (5) (2017) 470–487.
[13] B. Sang, Z.W. Li, X.H. Li, L.G. Yu, Z.J. Zhang, Graphene-based flame retardants: A review, *J. Mater. Sci.* 51 (18) (2016) 8271–8295.
[14] S. Bourbigot, S. Duquesne, Fire retardant polymers: Recent developments and opportunities, *J. Mater. Chem.* 17 (22) (2007) 2283–2300.
[15] M.M. Velencoso, A. Battig, J.C. Markwart, B. Schartel, F.R. Wurm, Molecular firefighting-how modern phosphorus chemistry can help solve the challenge of flame retardancy, *Angew. Chem. Int. Ed. Engl.* 57 (33) (2018) 10450–10467.
[16] S.Q. Huo, P.G. Song, B. Yu, S.Y. Ran, V.S. Chevali, L. Liu, Z.P. Fang, H. Wang, Phosphorus-containing flame retardant epoxy thermosets: Recent advances and future perspectives, *Prog. Polym. Sci.* 114 (2021) 101366.
[17] T. Liu, J. Jing, Y. Zhang, Z.P. Fang, Synthesis of a novel polyphosphate and its application with APP in flame retardant PLA, *RSC Adv.* 8 (8) (2018) 4483–4493.
[18] A.B. Morgan, The future of flame retardant polymers–unmet needs and likely new approaches, *Polym. Rev.* 59 (1) (2019) 25–54.
[19] X.L. Li, F.H. Zhang, R.K. Jian, Y.F. Ai, J.L. Ma, G.J. Hui, D.Y. Wang, Influence of eco-friendly calcium gluconate on the intumescent flame-retardant epoxy resin: Flame retardancy, smoke suppression and mechanical properties, *Compos. B Eng.* 176 (2019) 107200.

[20] H.Y. Ren, K.L. Qing, Y. Chen, Y.J. Lin, X. Duan, Smoke suppressant in flame retarded thermoplastic polyurethane composites: Synergistic effect and mechanism study, *Nano Res.* 14 (11) (2021) 3926–3934.
[21] M. Rajaei, D.Y. Wang, D. Bhattacharyya, Combined effects of ammonium polyphosphate and talc on the fire and mechanical properties of epoxy/glass fabric composites, *Compos. B Eng.* 113 (2017) 381–390.
[22] S.L. Qiu, C. Ma, X. Wang, X. Zhou, X.M. Feng, R.K.K. Yuen, Y. Hu, Melamine-containing polyphosphazene wrapped ammonium polyphosphate: A novel multifunctional organic-inorganic hybrid flame retardant, *J. Hazard. Mater.* 344 (2018) 839–848.
[23] M. Gao, S. Chen, H. Wang, Z.H. Chai, Design, preparation, and application of a novel, microencapsulated, intumescent, flame-retardant-based mimicking mussel, *ACS Omega* 3 (6) (2018) 6888–6894.
[24] M. Kim, H. Ko, S.M. Park, Synergistic effects of amine-modified ammonium polyphosphate on curing behaviors and flame retardation properties of epoxy composites, *Compos. B Eng.* 170 (2019) 19–30.
[25] W.T. He, P.G. Song, B. Yu, Z.P. Fang, H. Wang, Flame retardant polymeric nanocomposites through the combination of nanomaterials and conventional flame retardants, *Prog. Mater Sci.* 114 (2020) 100687.
[26] C.J. Shuai, L. Yu, P. Feng, C.D. Gao, S.P. Peng, Interfacial reinforcement in bioceramic/biopolymer composite bone scaffold: The role of coupling agent, *Colloids Surf. B Biointerfaces* 193 (2020) 111083.
[27] F. Ahangaran, A.H. Navarchian, Recent advances in chemical surface modification of metal oxide nanoparticles with silane coupling agents: A review, *Adv. Colloid Interface Sci.* 286 (2020) 102298.
[28] S. Kango, S. Kalia, A. Celli, J. Njuguna, Y. Habibi, R. Kumar, Surface modification of inorganic nanoparticles for development of organic-inorganic nanocomposites—A review, *Prog. Polym. Sci.* 38 (8) (2013) 1232–1261.
[29] H.J. Lin, H. Yan, B. Liu, L.Q. Wei, B.S. Xu, The influence of KH-550 on properties of ammonium polyphosphate and polypropylene flame retardant composites, *Polym. Degrad. Stab.* 96 (7) (2011) 1382–1388.
[30] Y.P. Sheng, Y.C. Wu, Y. Yan, H.C. Jia, Y.Y. Qiao, B.S. Underwood, D.Y. Niu, Y.R. Kim, Development of environmentally friendly flame retardant to achieve low flammability for asphalt binder used in tunnel pavements, *J. Clean. Prod.* 257 (2020) 120487.
[31] G.S. Liu, W.Y. Chen, J.G. Yu, A novel process to prepare ammonium polyphosphate with crystalline form II and its comparison with melamine polyphosphate, *Ind. Eng. Chem. Res.* 49 (23) (2010) 12148–12155.
[32] Y.J. Xie, C.A.S. Hill, Z.F. Xiao, H. Militz, C. Mai, Silane coupling agents used for natural fiber/polymer composites: A review, *Compos. A Appl. Sci. Manuf.* 41 (7) (2010) 806–819.
[33] Y. Tan, Z.B. Shao, L.X. Yu, J.W. Long, M. Qi, L. Chen, Y.Z. Wang, Piperazine-modified ammonium polyphosphate as monocomponent flame-retardant hardener for epoxy resin: Flame retardance, curing behavior and mechanical property, *Polym. Chem.* 7 (17) (2016) 3003–3012.
[34] L.B. Liu, Y. Xu, M.J. Xu, Z.Q. Li, Y.M. Hu, B. Li, Economical and facile synthesis of a highly efficient flame retardant for simultaneous improvement of fire retardancy, smoke suppression and moisture resistance of epoxy resins, *Compos. B Eng.* 167 (2019) 422–433.
[35] Y. Tan, Z.B. Shao, X.F. Chen, J.W. Long, L. Chen, Y.Z. Wang, Novel multifunctional organic-inorganic hybrid curing agent with high flame-retardant efficiency for epoxy resin, *ACS Appl. Mater. Interfaces* 7 (32) (2015) 17919–17928.
[36] Z.B. Shao, C. Deng, Y. Tan, L. Yu, M.J. Chen, L. Chen, Y.Z. Wang, Ammonium polyphosphate chemically-modified with ethanolamine as an efficient intumescent flame retardant for polypropylene, *J. Mater. Chem. A* 2 (34) (2014) 13955–13965.
[37] A.P. Hinckley, A.J. Muscat, Modified organosilane monolayers with enhanced radiation stability, *Langmuir* 36 (15) (2020) 4116–4122.
[38] M.H. Zhu, L. Liu, Z.Z. Wang, Mesoporous silica *via* self-assembly of nano zinc amino-tris-(methylenephosphonate) exhibiting reduced fire hazards and improved impact toughness in epoxy resin, *J. Hazard. Mater.* 392 (2020) 122343.
[39] Z.D. Zhang, J.Y. Qin, W.C. Zhang, Y.T. Pan, D.Y. Wang, R.J. Yang, Synthesis of a novel dual layered double hydroxide hybrid nanomaterial and its application in epoxy nanocomposites, *Chem. Eng. J.* 381 (2020) 122777.
[40] F. Fang, S.Y. Ran, Z.P. Fang, P.G. Song, H. Wang, Improved flame resistance and thermo-mechanical properties of epoxy resin nanocomposites from functionalized graphene oxide *via* self-assembly in water, *Compos. B Eng.* 165 (2019) 406–416.
[41] H.F. Pan, W. Wang, Y. Pan, L. Song, Y. Hu, K.M. Liew, Formation of layer-by-layer assembled titanate nanotubes filled coating on flexible polyurethane foam with improved flame retardant and smoke suppression properties, *ACS Appl. Mater. Interfaces* 7 (1) (2015) 101–111.
[42] Y.W. Yan, L. Chen, R.K. Jian, S. Kong, Y.Z. Wang, Intumescence: An effect way to flame retardance and smoke suppression for polystryene, *Polym. Degrad. Stab.* 97 (8) (2012) 1423–1431.
[43] Z. Li, A.J. González, V.B. Heeralal, D.Y. Wang, Covalent assembly of MCM-41 nanospheres on graphene oxide for improving fire retardancy and mechanical property of epoxy resin, *Compos. B Eng.* 138 (2018) 101–112.
[44] L. Costes, F. Laoutid, S. Brohez, P. Dubois, Bio-based flame retardants: When nature meets fire protection, *Mater. Sci. Eng. R Rep.* 117 (2017) 1–25.
[45] S.Q. Huo, S. Yang, J. Wang, J.W. Cheng, Q.Q. Zhang, Y.F. Hu, G.P. Ding, Q.X. Zhang, P.G. Song, H. Wang, A liquid phosphaphenanthrene-derived imidazole for improved flame retardancy and smoke suppression of epoxy resin, *ACS Appl. Polym. Mater.* 2 (8) (2020) 3566–3575.
[46] S. Yang, S.Q. Huo, J. Wang, B. Zhang, J.S. Wang, S.Y. Ran, Z.P. Fang, P.G. Song, H. Wang, A highly fire-safe and smoke-suppressive single-component epoxy resin with switchable curing temperature and rapid curing rate, *Compos. B Eng.* 207 (2021) 108601.
[47] J. Hong, T. Wu, H.Y. Wu, B.R. Zeng, S.N. Zeng, T. Chen, X. Wang, Z.W. Lu, C.H. Yuan, K. Balaji, D.F.S. Petri, L.Z. Dai, Nanohybrid silver nanoparticles@halloysite nanotubes coated with polyphosphazene for effectively enhancing the fire safety of epoxy resin, *Chem. Eng. J.* 407 (2021) 127087.
[48] F. Tuinstra, J.L. Koenig, Raman spectrum of graphite, *J. Chem. Phys.* 53 (3) (1970) 1126–1130.
[49] Z.L. Zhao, Q. Jin, N.E. Zhang, X.R. Guo, H. Yan, Preparation of a novel polysiloxane and its synergistic effect with ammonium polyphosphate on the flame retardancy of polypropylene, *Polym. Degrad. Stab.* 150 (2018) 73–85.
[50] X.S. Li, Z.L. Zhao, Y.H. Wang, H. Yan, X.Y. Zhang, B.S. Xu, Highly efficient flame retardant, flexible, and strong adhesive intumescent coating on polypropylene using hyperbranched polyamide, *Chem. Eng. J.* 324 (2017) 237–250.
[51] E. Desimoni, G.I. Casella, A.M. Salvi, T.R.I. Cataldi, A. Morone, XPS investigation of ultra-high-vacuum storage effects on carbon fibre surfaces, *Carbon* 30 (4) (1992) 527–531.
[52] W.C. Zhang, X.M. Li, R.J. Yang, Pyrolysis and fire behaviour of epoxy resin composites based on a phosphorus-containing polyhedral oligomeric silsesquioxane (DOPO-POSS), *Polym. Degrad. Stab.* 96 (10) (2011) 1821–1832.
[53] W.C. Zhang, X.M. Li, H.B. Fan, R.J. Yang, Study on mechanism of phosphorus-silicon synergistic flame retardancy on epoxy resins, *Polym. Degrad. Stab.* 97 (11) (2012) 2241–2248.
[54] M.S. Donley, D.R. Baer, T.G. Stoebe, Nitrogen 1s charge referencing for $Si_3N_4$ and related compounds, *Surf. Interface Anal.* 11 (6–7) (1988) 335–340.
[55] N.E. Zhang, J. Zhang, H. Yan, X.R. Guo, Q. Sun, R.J. Guo, A novel organic-inorganic hybrid K-HBPE@APP performing excellent flame retardancy and smoke suppression for polypropylene, *J. Hazard. Mater.* 373 (2019) 856–865.
[56] S.A. Kaluzhina, I.V. Sieber, Copper passivity and its breakdown in sodium bicarbonate solutions: A scanning electron microscopy and X-ray photoelectron and auger spectroscopy study, *Russ. J. Electrochem.* 42 (12) (2006) 1352–1357.
[57] Y.A. Guloyan, Colored glass: Technological and operational characteristics (review), *Glass Ceram.* 72 (9–10) (2016) 353–359.
[58] D.X. Liang, X.J. Zhu, P. Dai, X.Y. Lu, H.Q. Guo, H. Que, D.D. Wang, T. He, C.Z. Xu, H.M. Robin, Z.Y. Luo, X.L. Gu, Preparation of a novel lignin-based flame retardant for epoxy resin, *Mater. Chem. Phys.* 259 (2021) 124101.
[59] X.L. Hu, Y. Wang, J.R. Yu, J. Zhu, Z.M. Hu, Synthesis of a deoxybenzoin derivative and its use as a flame retardant in poly(trimethylene terephthalate), *J. Appl. Polym. Sci.* 135 (8) (2018) 45904.
[60] L.J. Li, Y.J. Chen, L.J. Qian, B. Xu, W. Xi, Addition flame-retardant effect of nonreactive phosphonate and expandable graphite in rigid polyurethane foams, *J. Appl. Polym. Sci.* 135 (10) (2018) 45960.
[61] L.J. Chen, L. Song, P. Lv, G.X. Jie, Q.L. Tai, W.Y. Xing, Y. Hu, A new intumescent flame retardant containing phosphorus and nitrogen: Preparation, thermal properties and application to UV curable coating, *Prog. Org. Coat.* 70 (1) (2011) 59–66.
[62] S.L. Qiu, X. Wang, B. Yu, X.M. Feng, X.W. Mu, R.K.K. Yuen, Y. Hu, Flame-retardant-wrapped polyphosphazene nanotubes: A novel strategy for enhancing the flame retardancy and smoke toxicity suppression of epoxy resins, *J. Hazard. Mater.* 325 (2017) 327–339.
[63] S.L. Qiu, W.Y. Xing, X.M. Feng, B. Yu, X.W. Mu, R.K.K. Yuen, Y. Hu, Self-standing cuprous oxide nanoparticles on silica@ polyphosphazene nanospheres: 3D nanostructure for enhancing the flame retardancy and toxic effluents elimination of epoxy resins via synergistic catalytic effect, *Chem. Eng. J.* 309 (2017) 802–814.
[64] P. Wang, Z.S. Cai, Highly efficient flame-retardant epoxy resin with a novel DOPO-based triazole compound: thermal stability, flame retardancy and mechanism, *Polym. Degrad. Stab.* 137 (2017) 138–150.